Impact of Time Dissemination Technologies on Synchrophasor Estimation Accuracy

A. Derviškadić, G. Frigo, M. Paolone
École Polytechnique Fédérale de Lausanne, 1015 Lausanne, Switzerland
mail: asja.derviskadic@epfl.ch

***Abstract*—The paper discusses the influence of the time synchronization technique on the synchrophasor estimation accuracy in modern Phasor Measurement Units (PMU). Specifically, we make reference to Global Positioning System (GPS), Precision Time Protocol (PTP) and White Rabbit time disseminations. The paper presents a PMU integrating the three technologies, and assess its performance in steady state conditions. The experimental validation demonstrates that the more deterministic the time source, the better the performance in terms of phase estimation accuracy.**

***Index Terms*—Phasor Measurement Unit (PMU), Synchrophasor network, Global Positioning System (GPS), Precision Time Protocol (PTP), White Rabbit, Allan deviation.**

I. Introduction

Synchrophasor technology represents one of the primary time-dependent applications used in modern power systems, as Phasor Measurement Units (PMUs) require an accurate and reliable time source to correctly phase align synchrophasors relative to geographically-distant substations [1], [2].

Typically, PMUs rely on the time reference made available by the Global Positioning System (GPS) that represents an optimal trade-off between performance and installation cost [3]. To improve timing redundancy and reliability, and given the potential vulnerability of GPS [4], mission-critical applications should use multiple timing sources, for instance deployable over the legacy power system telecommunication infrastructure [2]. In case the sky is not accessible and the telecommunication infrastructure is already available, there exist two possible network-based alternatives to substitute or support the GPS: the Precision Time Protocol (PTP) [5] and synchronous-Ethernet based systems like the White Rabbit (WR) Time Protocol [6]–[9].

The IEEE Std. C37.118.1 requires a maximum uncertainty in the synchrophasor time jitter of 1 μs [1], good-enough to correctly serve transmission applications. Distribution PMUs, requiring and increased level of accuracy, expect a lower level of uncertainty, in the order of tens of ns [2], [10]. Indeed, modern PMUs embed synchrophasor estimation algorithms exhibiting phase accuracies of few μrad, corresponding to 10 ns. In this context, the GPS provides an accuracy in the order of $\pm$100 ns when coupled with commercial receivers, whereas the PTP is characterized by an uncertainty of 1 μs. Therefore, these time references could negatively affect the phase estimation performance of the relative PMUs. Conversely, the WR achieves the sub-nanosecond, assuming only fiber interconnections and dedicated switches.

978-1-7281-1607-5/19/$31.00

The purpose of this paper is to assess the influence of the adopted time dissemination technique on the phase estimation accuracy. Specifically, we characterize the phase uncertainty of a PMU whose timing block integrates the GPS, the PTP and the WR technology. The phase stability is experimentally validated on the short, medium and long term, and the results are presented by means of the Allan deviation [11]. To carry out this analysis we use three PMUs that are based on the same hardware and on the same synchrophasor estimation algorithm, whereas we vary the time reference. Therefore, it is plausible to say that any discrepancy on the phase estimation accuracy comes from the adopted time synchronization module.

The paper is structured as follows. Section II describes the operating principles of the considered time dissemination techniques for PMU applications. Section III illustrates the implementation details of the developed PMU. Section IV assess its performance. Section V concludes the paper.

II. Time Synchronization Techniques for PMUs

A. Requirements

Time synchronization is a key factor in any PMU-based situational awareness system [2]. The IEEE Std. C37.118.1 [1] defines the phase of the synchrophasor as the instantaneous phase angle related to a cosine function at nominal power system frequency, and synchronized to Coordinated Universal Time (UTC). In that sense, any uncertainty in the time synchronization Δt linearly translates into a phase uncertainty $\Delta\varphi$, depending on the instantaneous frequency f of the signal:

$$\Delta\varphi = 2\pi f \Delta t + \varepsilon_{alg} + \varepsilon_{acq} \tag{1}$$

where ε_{alg} and ε_{acq} account for two other uncertainty sources, i.e., the phase error introduced by the adopted synchrophasor estimation algorithm and the phase noise produced by the acquisition process (e.g. due to quantization or nonlinear analog-to-digital conversion), respectively. In this paper, we assume these two contributions to be statistically independent and uncorrelated, and we focus mainly on the synchronization uncertainty, as its impact is expected to significantly exceed the other two in real-world operating conditions.

From the IEEE Std. it is possible to infer the maximum uncertainty on the synchrophasor time-jitter to be limited to 1 μs [1]. Indeed, this value is indirectly determined by the requirement for a maximum Total Vector Error (TVE) of 1%,

corresponding to a phase uncertainty of 0.01 rad in case the TVE is only influenced by the phase error. When time is the only source of error, this corresponds to 31 μs at 50 Hz, leading to the 10 times better recommended time uncertainty of 1 μs. However, it is well-established that PMUs operating in distribution networks are expected to meet more stringent accuracy requirements, at least two orders of magnitude lower than those met by transmission PMUs (TVE lower than 0.01%) [10], [12]. Therefore, the uncertainty contribution coming from the timing unit should be reduced to values in the order of tens of ns [2].

In the following, satellite- and network-based synchronization systems, that can be used for PMU applications, are briefly described. In this context, we make reference to their functional features, performance as well as applicability to the synchrophasor technology.

B. The Global Positioning System

In general, PMU applications rely on the GPS-based synchronization that is characterized by an accuracy in the order of $\pm$ 100 ns when coupled with commercial GPS receivers (e.g., [3]). In such a scenario, a dedicated GPS receiver must be installed in every PMU location, as well as in the Phasor Data Concentrator (PDC) in case time-stamping functionalities are implemented at data collection.

In order to properly lock satellites, though, the GPS receiver needs a clear view of the sky. The installation in enclosed spaces, as typical of high-rise urban environments, reduces the number of tracked satellites and determines signal reflections and wakening effects, resulting in a degradation of the time information accuracy [13]. Therefore, the GPS technology is not always the most suitable solution for PMU installations in urban areas or in substations without an ease access to the sky, such as underground substations.

C. The Precision Time Protocol

The Precision Time Protocol (PTP) was introduced by the IEEE Std. 1588 [5] and provides an accuracy of 1 μs, measured as the deviation of each node with respect to the UTC. The core element of the PTP is the exchange of time-tagged messages in a peer-to-peer link between master and slave clocks, used to calculate the link delay between the two clocks. PTP-aware routers composing the network implement the so-called hardware-assisted time-stamping, a technique to measure and compensate for the time spent by messages in queuing at their own ports. An extended profile for the use of PTP in power system applications is specified in [14] and, for instance, used in [15].

The first limitation of the PTP is represented by the assumption that the one-way delay is exactly half of the two-way delay, which is true only as long as the cable is very short. The second limitation is that the final PTP accuracy is limited by the precision and resolution of the master and slave clocks to measure the time when sending or receiving messages, typically equal to 100 ppm. The third limitation is that these clocks are typically free-running oscillators, without any guarantee of synchronism between oscillators at different nodes. This results in uncontrolled time drifts between masters and slaves. The higher the exchange rate of PTP messages, the lower the time drift, but also the higher the bandwidth needed for PTP-related traffic. Therefore, the predicted 1 μs accuracy, is rarely achieved in real-scale PTP deployments [16].

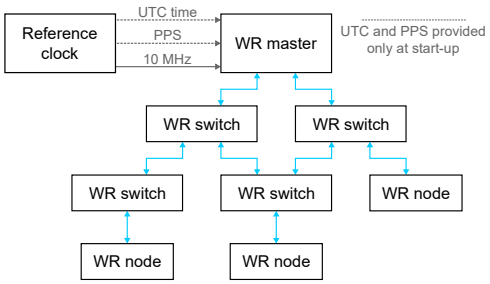

Fig. 1. White Rabbit network architecture.

D. The White Rabbit Protocol

The WR protocol has been developed and used at CERN to align the clocks of their particle accelerator complex [6], [17]. The protocol, enables the synchronization of thousands of devices connected in a network spanning several kilometers through already existing Ethernet-based networks. If we assume fiber interconnections, the time synchronization accuracy, measured as the deviation of each node with respect to the UTC, achieves the order of sub-nanosecond. Moreover, the protocol features a reliable and deterministic data delivery.

The WR is based on existing standards, namely Ethernet (IEEE 802.3) [18], Synchronous Ethernet (SyncE) [19], and IEEE 1588 (PTPv2) [5], and adopts a technique called Precise Phase Measurement [20]. The combination of these technologies, enables the achievement of the sub-nanosecond accuracy.

Figure 1 shows the layout of a typical WR network, that is composed of WR nodes and WR switches, interconnected by fiber or copper links. Data-wise, it is a standard Ethernet switched network, i.e., there is no hierarchy: any node can talk to any other node in the network. Regarding time synchronization, there is a hierarchy, that goes from the top, i.e., from the WR master, down to other WR switches and consequently nodes. The WR switch, key element of any WR network, is similar to a standard Ethernet switch, but it is also able to precisely distribute the WR master clock over the network thanks to a technique called Precise Phase Measurement.

This technology represents an appropriate and effective alternative or complement to the GPS with particular focus on the cases when (i) the sky is not accessible (e.g., urban areas), (ii) the telecommunication infrastructure is already available, and (iii) the typical length between two PMUs is less than 10 km (e.g., sub transmission or power distribution networks).

III. The Developed PMU

In order to characterized the influence of the adopted time synchronization technique on the synchrophasor estimation accuracy, we develop a PMU that can be synchronized to the

absolute time reference with three different sources, i.e., the GPS, the PTP and the WR. To carry out the analysis, we use three separate PMUs. However, in order to guarantee a fair and rigorous performance comparison, we replicate all the building blocks that have an impact on the phase estimation for the three devices. Specifically, to avoid any influence introduced by the sampling process, we use the same hardware platform (see Section III-A); to limit any discrepancy introduced by the synchrophasor estimation process, we use the same software (see Section III-B). We perform the tests, by switching among the three timing units: it is thus reasonable to say that any difference among the synchrophasor estimates is related to the adopted time dissemination technique.

In this regard, the so-called GPS-PMU relies on the GPS receiver only, the PTP-PMU is based on PTP, whereas the WR-PMU implements the WR protocol. As regards the synchrophasor estimation process, we consider the Enhanced Interpolated DFT (e-IpDFT) approach, already implemented in a PMU device [3] and compliant with all the requirements for protection class PMUs. Any difference or similarity is further illustrated in the remainder of this Section, with a focus on all implementation details that might condition time accuracy.

A. The Hardware Platform

The architecture of the designed PMU is based on the National Instruments (NI) compactRIO (cRIO) system, an embedded industrial controller with a real-time processor, a user-programmable Field Programmable Gate Array (FPGA) and reconfigurable IO modules. The FPGA is equipped with a free-running 40 MHz clock. The three main processes, i.e., (i) PMU time synchronization, (ii) signal acquisition and (iii) synchrophasor estimation, run at the FPGA level. The main added value of FPGAs is that calculations are executed with a high determinism governed by the FPGA on-board clock, that is a fundamental feature for time-critical applications.

The GPS-PMU, described in [3], is based on the cRIO-9068 controller, embedding a reconfigurable Xilinx Zynq 7020 FPGA with an on-board clock frequency of 40 MHz, 106400 flip-flops, 53200 look-up tables (LUTs), 4480 kbits of block RAM and 220 DSP slices (each one characterized by a 25 X 18 multiplier, an adder and an accumulator) [21]. The UTC-GPS signal is acquired by means of the NI 9467 GPS time-stamping and synchronization module, that is directly coupled with the on-board FPGA clock, enabling the timestamping of each tick of the 40 MHz clock with real-world time, accurate to within $\pm$ 100 ns. The GPS module is coupled with a Trimble's Bullet III GPS receiver, an active GPS antenna with a high-gain preamplifier and dual passband filters [22].

The PTP-PMU is based on the cRIO-9039 controller, characterized by a reconfigurable Xilinx Kintex-7 FPGA with an on-board clock frequency of 40 MHz, 407600 flip-flops, 203800 LUTs, 16020 kbits of block RAM and 840 DSP slices. The PTP distribution is achieved thanks to the NI TimeSync library, that synchronizes the timekeeping clocks of the cRIO with an accuracy of $\pm$ 1 μs. It is worth to point out that the FPGA clock is locked to the UTC-PTP. The UTC-PTP reference signal is acquired via a point-to-point connection to the master clock Network Time Server 100 manufactured by Tekron [23]. The latter is further coupled with a GPS receiver to retrieve the absolute time information.

The WR-PMU, described in [24], is based on the same hardware platform as the GPS-PMU, i.e., cRIO-9068. The WR-UTC signal is provided by the NI WR cRIO module, equipped with a Xilinx Spartan-6 FPGA [25]. The module is operated in slave mode, and is connected point-to-point via a fiber link to a WR switch by Seven Solutions operated in grand-master mode [26]. The latter is connected to a Windows machine providing the Network Time Protocol (NTP) service used to determine the absolute time at reboot. The workstation embeds a Meinberg 180 PEX card (further coupled with a GPS receiver) that disciplines the NTP service and generates reference PPS and 10 MHz signals, fed to the WR switch [27]. As discussed in [24], the WR cRIO is characterized by two hardware limitations: (i) the UTC-WR polling is limited by the module's FPGA clock running at 50 kHz, thus providing a discrete time reference and (ii) the UTC-WR reading introduces a deterministic delay. In order to overcome to these limitations the WR-PMU embeds a free running clock conditioned by a PI controller, that provides improved time resolution (25 ns, i.e., the FPGA tick) and compensates for the reading time delay.

The sampling of the voltage and current waveforms is realized by means of two parallel 24-bits delta–sigma converters, module NI 9225 and 9227 respectively, characterized by a sampling rate F_s of 50 kHz and an input range of 300 V_{RMS} for the voltage and 5 A_{RMS} for the current.

B. The Synchrophasor Estimation Algorithm

As aforementioned, the developed PMU adopts the e-IpDFT to estimate the synchrophasor amplitude $\hat{A}$ and phase angle $\hat{\varphi}_0$, the frequency $\hat{f}$, and the Rate-of-Change-of-Frequency (ROCOF) associated to the fundamental component of the power signal under analysis. This technique, described in Algorithm 1, is specifically designed to mitigate the effects of long-range spectral leakage produced by the negative image of the fundamental component.

Algorithm 1 The e-IpDFT synchrophasor estimation.

1: $x[n] := \{x(t_n) \quad | \quad t_n = nT_s,\ n = [0, \dots N-1] \in \mathbb{N}\}$
2: $X(k) = \texttt{DFT}(x[n] \cdot w[n])$
3: $\{\widehat{f}^0, \widehat{A}^0, \widehat{\varphi}_0^0\} = \texttt{IpDFT}(X(k))$
4: **for** $p = 1 \rightarrow P$
5: $\quad \widehat{X}^{p-}(k) = \texttt{wf}(-\widehat{f}^{p-1}, \widehat{A}^{p-1}, -\widehat{\varphi}_0^{p-1})$
6: $\quad \widehat{X}^{p+}(k) = X(k) - \widehat{X}^{p-}(k)$
7: $\quad \{\widehat{f}^p, \widehat{A}^p, \widehat{\varphi}_0^p\} = \texttt{IpDFT}(\widehat{X}^{p+}(k))$
8: **end for**

First, the PMU acquires a discrete time-series of samples $x[n]$, where $x(t)$ is the time-variant power system signal under analysis, N is the number of samples that compose the considered observation interval and $F_s = T_s^{-1}$ is the sampling rate (line 1). The signal is windowed with the Hanning

function $w[n]$ to reduce long-range spectral leakage effects, then the weighted signal DFT $X(k)$ is computed (line 2).

A preliminary estimate of the fundamental parameters is obtained by processing the highest DFT bins via the IpDFT technique (line 3) [28], [29]. Specifically, the fractional correction term δ, indicating the location of the actual signal frequency with respect to the location of the highest amplitude bin k_m, is calculated as follows:

$$\delta = \varepsilon \cdot \frac{2 \cdot |X(k_m + \varepsilon)| - |X(k_m)|}{|X(k_m + \varepsilon)| + |X(k_m)|} \tag{2}$$

The latter is used to estimate the fundamental component parameters based on the following expressions:

$$\hat{f} = (k_m + \delta)\Delta f \tag{3}$$

$$\hat{A} = |X(k_m)| \left| \frac{\pi\delta}{\sin(\pi\delta)} \right| |\delta^2 - 1| \tag{4}$$

$$\hat{\varphi}_0 = \angle X(k_m) - \pi\delta \tag{5}$$

These values enable us to reconstruct the component's negative image $\widehat{X}^-(k)$, whose analytic expression is known for the Hanning window function (line 5). The negative image is subtracted from the original DFT bins, that now should account only for the fundamental component's positive image $\widehat{X}^+(k)$ (line 6). Finally, the IpDFT is applied to such spectrum, resulting in an enhanced estimation of the fundamental tone parameters $\{\hat{f}, \hat{A}, \hat{\varphi}_0\}$ (line 7).

It is worth observing that the compensation of the spectral interference produced by the negative image of the fundamental component, can be repeated a predefined number of times P. In the PMU described in [3], the procedure was repeated only once. More recent findings have demonstrated that setting P equal to 2 enables us to significantly improve the e-IpDFT estimation accuracy [30]. Therefore, in the developed PMU, this compensation routine is performed twice.

In this way, we aim at minimizing the uncertainty contribution due to the synchrophasor estimation algorithm. In this regard, Fig. 2 compares the phase estimation errors obtained with P equal to 1 and 2, for a simulated waveform in steady-state test condition. For this analysis, we set the fundamental amplitude and initial phase equal to 1 pu and 0 rad, respectively, whereas we vary the fundamental frequency between 47.5 and 52.5 Hz, i.e., within the PMU pass-bandwidth. In order to reproduce a plausible measurement noise, the waveform is corrupted by an additive uncorrelated white Gaussian noise, whose variance is scaled to reproduce an overall signal-to-noise ratio (SNR) of 85 dB, coherently with the noise level measured on the experimentally acquired test waveforms in Section IV. In this context, it is interesting to observe that the second iteration provides a significant performance enhancement in case of non-nominal frequency values, with a phase error not exceeding 5 μrad.

As a result, looking at the uncertainty balance in Eq. (1), we are now able to quantify both ε_{alg} and ε_{acq}. The synchrophasor estimation uncertainty ε_{alg} is rather constant in the considered spectral bandwidth and keeps 5 μrad, whereas

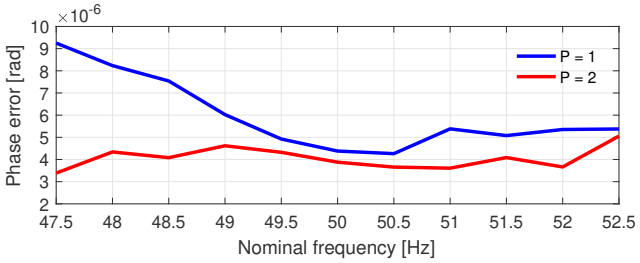

Fig. 2. Phase estimation error as provided by e-IpDFT as function of the fundamental frequency, when the iteration number P of the compensation routine is set equal to 1 (blue) and 2 (red), respectively. The additive white Gaussian noise produces a signal-to-noise ratio of 85 dB.

the measurement noise exceeds the quantization noise of any modern acquisition front end and thus makes negligible its uncertainty contribution ε_{acq}.

The measurements are reported by the PMU with reporting rate F_r of 50 frames per second (fps) and are time-tagged with the so-called time-stamp. The e-IpDFT adopts an observation interval T of 60 ms and a 50 kHz sampling frequency $F_s = 1/T_s$ (leading to 3000-point windows).

C. The Free-Running Sampling Process

Regardless of the adopted time dissemination technique, the sampling process of the waveforms is free-running and is described in [3]: at the FPGA level, we derive from the UTC-PPS signal a sub PPS square waveform (hereafter called subPPS), locked to the UTC-PPS and characterized by a frequency corresponding to the PMU reporting rate F_r. The signal acquisition, the synchrophasor estimation, and the synchrophasor time-stamping are triggered by the rising edge of such subPPS.

Then, a time refinement is performed *a posteriori*, taking into account two delays. First, the sampling frequency might drift from its nominal value, due to oscillator degradation or environment conditions (such as the room temperature). Second, the subPPS and the sampling process might not be exactly locked to each other. The developed PMU measures those delays and compensates for them by updating frequency and phase estimations (see [3] for further details).

IV. Performance Assessment

The phase accuracy of the described time dissemination technologies has been experimentally validated with respect to the steady-state test conditions of the IEEE Std. C37.118.1 [1]. For this analysis, we employed a dedicated PMU calibrator [31], that generates user-defined voltage test waveforms, simultaneously reacquires them, and extracts the reference values of fundamental amplitude, frequency and initial phase through a nonlinear least-square optimization routine. This operating procedure, thoroughly described in [32], has been proven to provide a unique and robust solution within the whole range of static tests required by [1], with a worst-case TVE in the order of 4×10^{-4}%.

In this context, Fig. 3 presents the measurement setup specifically designed for the PMUs' performance assessment.

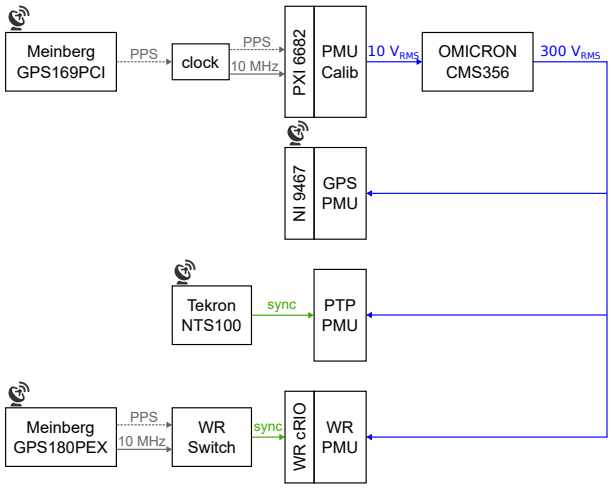

Fig. 3. Measurement setup for the assessment of the PMUs' phase estimation accuracy. The PMU calibrator generates the user-defined test waveforms, that are amplified up to 300 V by the CMS 356 OMICRON amplifier, and then supplied to the three considered PMUs, relying on GPS, PTP and WR time dissemination, respectively.

The PMU calibrator consists of a NI PXI 1042Q (National Instruments, Austin, TX), supplied with three operating modules: the NI PXI-8110 embedded controller, the NI PXI-6682 synchronization board, and the NI PXI-6289 data acquisition (DAQ) board. The internal trigger is provided by the FS725 rubidium oscillator (Stanford Research Systems, Sunnyvale, CA), disciplined by the GPS 169-PCI Radio Clock (Meinberg, Bad Pyrmont). This peculiar synchronization scheme enables us to exploit the advantages of both time-sources: the rubidium oscillator provides a reduced short-term variability on the 10 MHz time-base signal, whereas the GPS clock guarantees the alignment with respect to UTC and minimizes the long-term variability, as experimentally validated in [31].

As aforementioned, the DAQ board allows for generating and simultaneously re-acquiring the voltage waveforms provided to the PMUs under test. To this end, the generation stage employs three 16-bits digital-to-analog converters (DACs) with an output range of ± 10 V and a sampling frequency of 500 kHz, whereas the acquisition stage digitizes the same waveforms by means of a multiplexed 18-bits analog-to-digital converter (ADC) with an input range of ± 10 V and a sampling frequency of 100 kHz. In order to minimize any uncertainty due to the internal time-source and the data acquisition process, also the phase displacement introduced by the multiplexer has been characterized and compensated.

In this paper, we consider a steady-state test waveform, consisting of a single fundamental tone whose amplitude and initial phase are set equal to 10 V and 0 rad, respectively, whereas the frequency ranges between 47.5 and 52.5 Hz, i.e., within the expected pass-bandwidth of a PMU with a nominal frequency of 50 Hz and a reporting rate of 50 fps.

Before being supplied to the PMUs under test, the voltage waveforms are amplified by the CMS-356 OMICRON amplifier with a fixed gain of 30. The combined effect of DAQ board and voltage amplifier introduces a limited measurement noise, with an overall SNR equal to 85 dB.

Based on the IEEE Std. C37.118.1 requirements, the PMU estimation uncertainty should be evaluated in terms of Total Vector Error, Frequency Error, and ROCOF Error. Nevertheless, it is worth noticing that the synchrophasor phase angle is the quantity more directly affected by a poor synchronization performance. For this reason, the present analysis focuses specifically on the phase estimation error, that accounts for two main uncertainty contributions, i.e., the synchrophasor estimation algorithm and the time dissemination technology. In this regard, it should be noticed that, since the three PMUs implement the same e-IpDFT algorithm, the first contribution can be reasonably considered as coincident. As a consequence, the different performance should be related primarily to the adopted time dissemination technology.

For each PMU configuration, we evaluate the phase estimation accuracy over a test duration of 24 hours, as function of the fundamental frequency. In this context, the performance comparison relies on two quantitative indexes. On one side, we evaluate the cumulative distribution functions (CDFs) associated to the obtained phase errors. Since the sampling process might not be locked to the actual fundamental frequency and thus introduce a phase drift in the PMU estimates, we first normalize the phase errors by their mean value over the entire test duration, then we perform a histogram analysis, and finally we extract the CDF. In this way, we are able to compensate any linear drift and estimate a statistical distribution that accounts only for the actual phase variability.

On the other side, we compute the Allan deviation that quantifies the estimation uncertainty specifically related to the stability of the adopted time dissemination technology [11]. To this end, we consider the M-sample variance, defined as follows:

$$\sigma^2(\tau) = \frac{1}{M-1}\left[\sum_{m=0}^{M-1}\delta_\varphi^2(m,\tau) - \frac{1}{M}\left(\sum_{m=0}^{M-1}\delta_\varphi(m,\tau)\right)^2\right]$$
$$\delta_\varphi(m,\tau) = \frac{\varphi(mT_r+\tau)-\varphi(mT_r)}{\tau} \quad (6)$$

where $\varphi(mT_r)$ is the phase estimate associated to mT_r time instant, expressed as function of the reporting period T_r, M is the sample number for the variance computation, and τ is the time deviation between two consecutive phase estimates. In this context, the Allan deviation is simply its square root.

In order to evaluate the phase estimation accuracy over different time intervals, we vary τ between 10^1 to 10^4 s. In this way, we are able to compare both the short- and long-term stability of the considered time dissemination technologies.

It is worth to point out that, as highlighted in Fig. 3, the master clocks of the PMUs and the one of the PMU calibrator use separate GPS receivers, thus guaranteeing the non correlation among the various absolute times.

In the following paragraphs, we consider two different scenarios. The first one represents a plausible normal operating condition and thus accounts for the expected performance

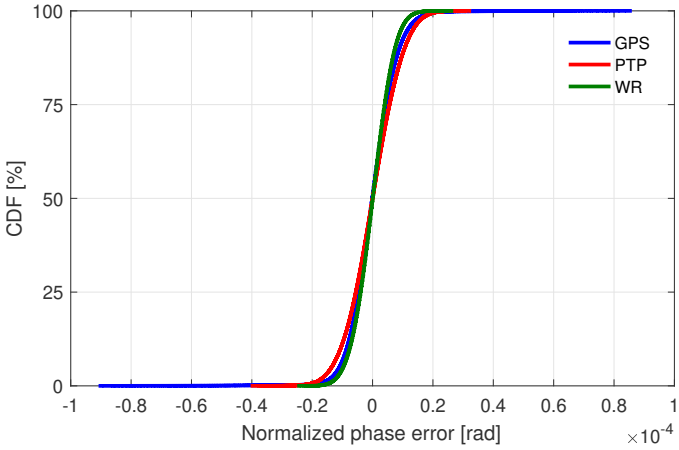

Fig. 4. Phase error cumulative distribution functions as provided by GPS (blue), PTP (red) and WR (green) PMUs over a test duration of 24 hours. The test waveform consists of a single fundamental tone whose amplitude, frequency and phase are set equal to 300 V, 50 Hz, and 0 rad, respectively.

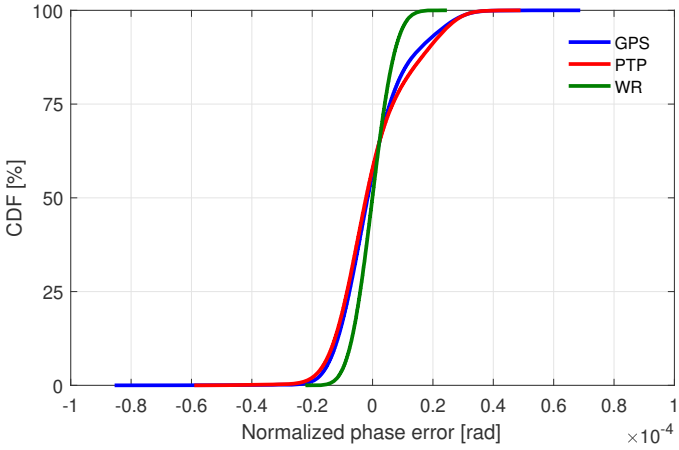

Fig. 5. Phase error cumulative distribution functions as provided by GPS (blue), PTP (red) and WR (green) PMUs over a test duration of 24 hours. The test waveform consists of a single fundamental tone whose amplitude, frequency and phase are set equal to 300 V, 47.5 Hz, and 0 rad, respectively.

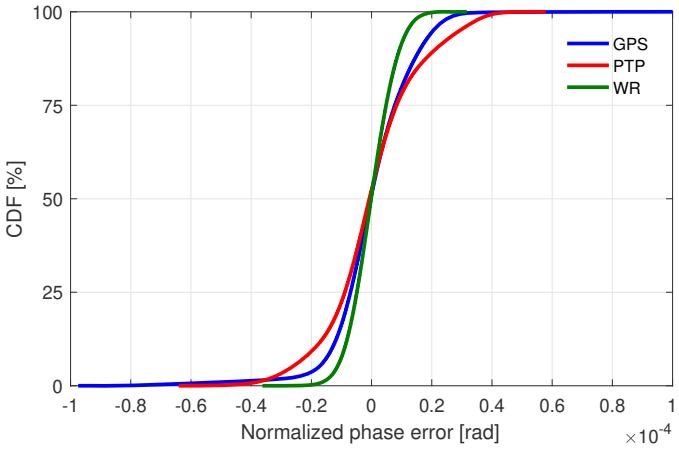

Fig. 6. Phase error cumulative distribution functions as provided by GPS (blue), PTP (red) and WR (green) PMUs over a test duration of 24 hours. The test waveform consists of a single fundamental tone whose amplitude, frequency and phase are set equal to 300 V, 52.5 Hz, and 0 rad, respectively.

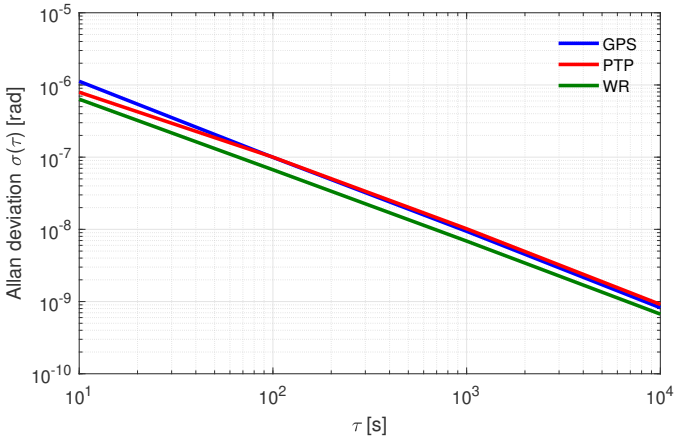

Fig. 7. Phase error Allan deviation as function of the time interval τ, for GPS (blue), PTP (red) and WR (green) PMUs over a test duration of 24 hours. The test waveform consists of a single fundamental tone whose amplitude, frequency and phase are set equal to 300 V, 50 Hz, and 0 rad, respectively.

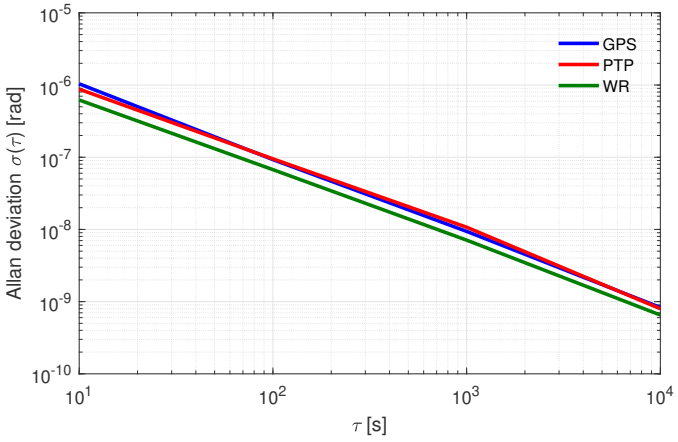

Fig. 8. Phase error Allan deviation as function of the time interval τ, for GPS (blue), PTP (red) and WR (green) PMUs over a test duration of 24 hours. The test waveform consists of a single fundamental tone whose amplitude, frequency and phase are set equal to 300 V, 47.5 Hz, and 0 rad, respectively.

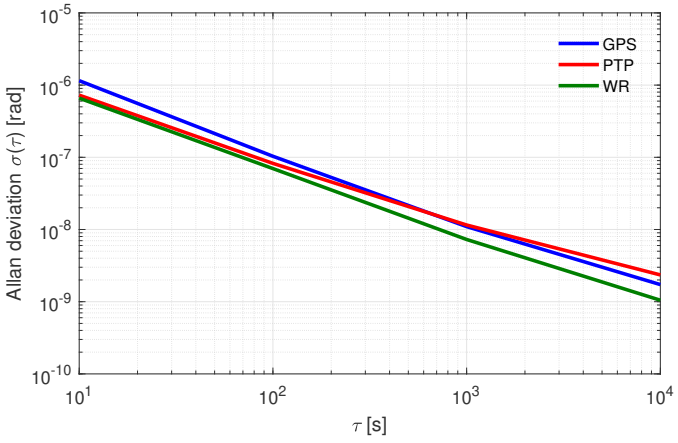

Fig. 9. Phase error Allan deviation as function of the time interval τ, for GPS (blue), PTP (red) and WR (green) PMUs over a test duration of 24 hours. The test waveform consists of a single fundamental tone whose amplitude, frequency and phase are set equal to 300 V, 52.5 Hz, and 0 rad, respectively.

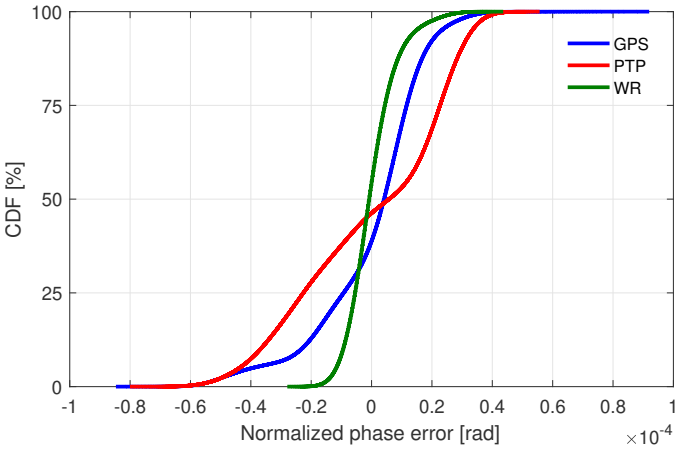

Fig. 10. Worst-case scenario: phase error cumulative distribution function over a 24-hour test, for GPS (blue), PTP (red) and WR (green) PMUs. The test waveform consists of a single fundamental tone whose amplitude, frequency and phase are set equal to 300 V, 50 Hz, and 0 rad, respectively.

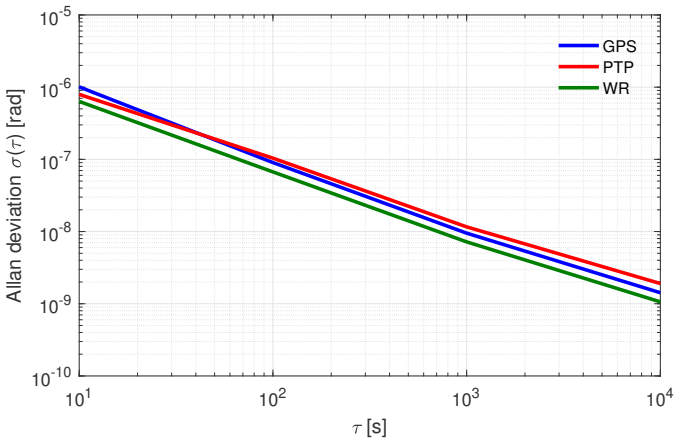

Fig. 11. Worst-case scenario: phase error Allan deviation over a 24-hour test, for GPS (blue), PTP (red) and WR (green) PMUs. The test waveform consists of a single fundamental tone whose amplitude, frequency and phase are set equal to 300 V, 50 Hz, and 0 rad, respectively.

of the three PMU configurations, whereas the second one determines the worst-case condition, in order to assess the maximum phase uncertainty that can be introduced by GPS, PTP and WR synchronization schemes.

A. Normal Operating Conditions

In the first test, we compare the phase estimation accuracy obtained in normal operating conditions as function of the fundamental frequency. In this context, Fig. 4, 5 and 6 present the phase error CDFs for 50, 47.5 and 52.5 Hz, respectively.

Independently from the fundamental frequency values, the WR enables us to keep the normalized phase error within ± 15 μrad, whereas PTP and GPS might exceed 30 μrad. It is also worth observing that the GPS tends to outperform the PTP and this performance discrepancy becomes more evident, as we consider non-nominal test conditions, when the sampling rate is not locked to the fundamental frequency.

In the same test conditions, we evaluate the Allan deviation as function of the time interval τ (see Fig. 7, 8 and 9). Coherently with the previous results, we notice how the WR is characterized by the lowest variability, whereas PTP and GPS provide comparable performance. For instance, at 50 Hz the WR Allan deviation decreases from 0.5 μrad up to 0.7 nrad, if we enlarge the time interval from 10^1 up to 10^4 s. This performance enhancement provided by the WR time dissemination becomes more significant as τ increases, particularly when asynchronous sampling conditions are considered.

B. Worst-Case Operating Conditions

Given a fundamental frequency of 50 Hz[1], we carried out a series of repeated experiments in order to verify the stability over time of the considered accuracy indexes. Within this dataset, we extract the worst-case performance associated to each time dissemination and compare them in order to experimentally determine the accuracy limit provided by GPS, PTP and WR-PMUs.

As shown in Fig. 10, the CDFs might vary significantly as function of the adopted synchronization sources. Once more, the WR provides the best performance, with a phase error limited within ± 16 μrad, i.e., comparable with the results in normal operating conditions. Conversely, both PTP and GPS exhibit a significant performance degradation with phase errors exceeding 50 μrad. In particular, the worst-case is represented by the PTP-PMU, whose CDF is characterized by a wider range of values and is not centered around 0 rad.

Similar considerations hold also for the Allan deviations presented in Fig. 11. Independently from the considered time interval τ, the WR confirms to be characterized by a lower phase variability (equal to 1 nrad at 10^4 s), whereas PTP and GPS provide nearly coincident performance.

In Table I, we report the main features of the phase error statistical distributions obtained in both normal and worst-case operating conditions. For each time dissemination technique and fundamental frequency value, we compute the minimum and maximum phase error, as well as its standard deviation. In all the considered configurations, the WR outperforms PTP and GPS, with a worst-case standard deviation of 8.1 μrad. In this regard, it is worth noticing how the WR synchronization produces a phase variability that is comparable with the synchrophasor accuracy limit (i.e., 5 μrad). In other words, the WR-PMU is capable of minimizing the time dissemination uncertainty contribution and thus optimizing the performance of the actual synchrophasor estimation algorithm.

V. Conclusion

In this paper, we discuss the uncertainty contribution of the time dissemination technology on the synchrophasor estimation in PMU applications. To this end, we carry out a performance comparison campaign, where we consider the same hardware platform (NI-cRIO) and synchrophasor estimation

[1]The choice of limiting the analysis to a synchronous sampling condition enables us to limit the other uncertainty sources and focus primarily on the stability time synchronization source.

TABLE I
PHASE ERROR [μRAD]- STATISTICAL DISTRIBUTION FEATURES

		Normal			Worst-Case
		47.5 Hz	50 Hz	52.5 Hz	50 Hz
GPS	min	-85.5	-90.8	-97.5	-84.7
	max	68.8	85.9	109.2	92.0
	std	11.3	7.4	13.3	18.1
PTP	min	-59.1	-40.4	-64.1	-80.1
	max	49.0	32.6	57.8	55.7
	std	12.3	8.2	15.7	25.9
WR	min	-22.2	-25.0	-36.3	-27.9
	max	24.6	26.7	31.6	43.6
	std	5.9	5.8	7.1	8.1

algorithm (e-IpDFT), whereas we vary three different time synchronization sources, i.e., GPS, PTP and WR. By means of experimental tests, we evaluate each configuration accuracy and stability in terms of phase estimation error.

For a more rigorous performance characterization, we quantify the cumulative distribution functions as well as the Allan deviations associated to the phase errors provided by each PMU configuration. On one side, we characterize the cumulative distribution function in terms of error minimum, maximum and standard deviation. On the other side, the Allan deviation enables us to evaluate the estimation stability over different time intervals, ranging from 10^1 up to 10^4 s.

The proposed analysis confirms that the time dissemination technique significantly affects the synchrophasor estimation accuracy. In particular, the WR protocol proves to guarantee a noticeable performance enhancement, independently from the considered fundamental frequency and time interval. In the worst-case, the WR synchronization produces a phase variability of 8.1 μrad that is comparable with the synchrophasor accuracy limit (i.e., 5 μrad). In other words, the WR-PMU is capable of minimizing the time dissemination uncertainty contribution and thus optimizing the performance of the actual synchrophasor estimation algorithm.

REFERENCES

[1] "IEEE Standard for Synchrophasor Measurements for Power Systems," *IEEE Std C37.118.1-2011 (Revision of IEEE Std C37.118-2005)*, pp. 1–61, Dec 2011.

[2] "Time synchronization in the electric power system," *NASPI Time Synchronization Task Force*, 2017.

[3] P. Romano and M. Paolone, "Enhanced interpolated-DFT for synchrophasor estimation in FPGAs: Theory, implementation, and validation of a PMU prototype," *IEEE Transactions on Instrumentation and Measurement*, vol. 63, no. 12, pp. 2824–2836, Dec 2014.

[4] X. Jiang, J. Zhang, B. J. Harding, J. J. Makela, A. D. Domı *et al.*, "Spoofing GPS receiver clock offset of phasor measurement units," *IEEE Transactions on Power Systems*, vol. 28, no. 3, pp. 3253–3262, 2013.

[5] "IEEE Standard for a Precision Clock Synchronization Protocol for Networked Measurement and Control Systems," *IEEE Std 1588-2008 (Revision of IEEE Std 1588-2002)*, pp. 1–300, July 2008.

[6] J. Serrano, P. Alvarez, M. Cattin, E. G. Cota, P. M. J. H. Lewis, T. Włostowski *et al.*, "The white rabbit project," in *Proceedings of ICALEPCS TUC004, Kobe, Japan*, 2009.

[7] M. Lipiński, E. van der Bij, J. Serrano, T. Włostowski, G. Daniluk, A. Wujek, M. Rizzi, and D. Lampridis, "White rabbit applications and enhancements," in *Proceedings of ISPCS 2018*, Oct 2018, pp. 1–4.

[8] F. Ramos, J. L. Gutiérrez-Rivas, J. López-Jiménez, B. Caracuel, and J. Díaz, "Accurate timing networks for dependable smart grid applications," *IEEE Transactions on Industrial Informatics*, vol. 14, no. 5, pp. 2076–2084, May 2018.

[9] A. Dhananjay and et Al., "Measurement tools for substation equipment: Testing the interoperability of time transfer and communications protocols," in *Proceedings of ISPCS 2018*, Oct 2018, pp. 1–4.

[10] "Synchrophasor monitoring for distribution systems: Technical foundations and applications," *NASPI Distribution Task Team*, 2018.

[11] D. W. Allan, "Statistics of atomic frequency standards," *Proceedings of the IEEE*, vol. 54, no. 2, pp. 221–230, Feb 1966.

[12] P. Romano, "DFT-based synchrophasor estimation algorithms and their integration in advanced phasor measurement units for the real-time monitoring of active distribution networks," *EPFL PhD dissertation*, 2016.

[13] E. Costa, "Simulation of the effects of different urban environments on GPS performance using digital elevation models and building databases," *IEEE Transactions on Intelligent Transportation Systems*, vol. 12, no. 3, pp. 819–829, Sept 2011.

[14] "IEEE Standard Profile for Use of IEEE 1588 Precision Time Protocol in Power System Applications," *IEEE Std C37.238-2017 (Revision of IEEE Std C37.238-2011)*, pp. 1–42, June 2017.

[15] H. F. Albinali and A. P. S. Meliopoulos, "Resilient protection system through centralized substation protection," *IEEE Transactions on Power Delivery*, vol. 33, no. 3, pp. 1418–1427, June 2018.

[16] M. Lipiński, T. Włostowski, J. Serrano, and P. Alvarez, "White rabbit: a PTP application for robust sub-nanosecond synchronization," in *Proceedings of ISPCS 2011*, 2011, p. 25–30.

[17] CERN, "The White Rabbit Project," 2017, accessed: 2018-10-01. [Online]. Available: http://white-rabbit.web.cern.ch/

[18] "IEEE Standard for Ethernet," *IEEE Std 802.3-2015 (Revision of IEEE Std 802.3-2012)*, pp. 1–4017, March 2016.

[19] "Timing Characteristics of Synchronous Ethernet Equipment Slave Clock (EEC)," *ITU-T Rec. G.8262*, August 2007.

[20] G. Daniluk and T. Włostowski, "White rabbit: Sub-nanosecond synchronization for embedded systems," in *43rd Annual Precise Time and Time Interval Systems and Applications Meeting*, Nov 2011.

[21] "National instruments CompactRIO controller," accessed: 2018-10-01. [Online]. Available: http://www.ni.com/en-us/shop/select/compactrio-controller

[22] "Trimble bullet III GPS antenna," accessed: 2018-10-01. [Online]. Available: https://www.trimble.com/timing/bullet-gps-antenna.aspx

[23] "Tekron NTS100," accessed: 2018-10-01. [Online]. Available: https://tekron.com/news/release/tekron-nts100-network-time-server-new-product

[24] R. Razzaghi, A. Derviškadić, and M. Paolone, "A white rabbit synchronized PMU," in *2017 IEEE PES Innovative Smart Grid Technologies Conference Europe (ISGT-Europe)*, Sept 2017, pp. 1–6.

[25] "CompactRIO white rabbit (CRIO-WR)," accessed: 2018-10-01. [Online]. Available: https://www.ohwr.org/projects/crio-wr/wiki

[26] "Seven solutions white rabbit switch," accessed: 2018-10-01. [Online]. Available: http://sevensols.com/index.php/products/white-rabbit-switch/

[27] "Meinberg GPS180PEX: Low profile GPS clock," accessed: 2018-10-01. [Online]. Available: https://www.meinbergglobal.com/english/products/pci-express-gps-clock.htm

[28] V. K. Jain, W. L. Collins, and D. C. Davis, "High-accuracy analog measurements via interpolated FFT," *IEEE Transactions on Instrumentation and Measurement*, vol. 28, no. 2, pp. 113–122, 1979.

[29] T. Grandke, "Interpolation algorithms for Discrete Fourier Transforms of weighted signals," *IEEE Transactions on Instrumentation and Measurement*, vol. 32, no. 2, pp. 350–355, 1983.

[30] A. Derviškadić, P. Romano, and M. Paolone, "Iterative-interpolated DFT for synchrophasor estimation: A single algorithm for P- and M-class compliant PMUs," *IEEE Transactions on Instrumentation and Measurement*, vol. 67, no. 3, pp. 547–558, March 2018.

[31] G. Frigo, A. Derviškadić, D. Colangelo, J.-P. Braun, and M. Paolone, "Characterization of uncertainty contributions in a high-accuracy PMU validation system," *Measurement*, 2018.

[32] G. Frigo, D. Colangelo, A. Derviškadić, M. Pignati, C. Narduzzi, and M. Paolone, "Definition of accurate reference synchrophasors for static and dynamic characterization of PMUs," *IEEE Transactions on Instrumentation and Measurement*, vol. 66, no. 9, Sept 2017.